(Preprint) AAS 15-365

CENTROID DYNAMICS FOR GROUP OBJECT TRACKING

Christopher Binz* **and Liam Healy***

Immediately following a scenario like a CubeSat deployment, the presence of multiple objects in close proximity makes the observation assignment problem—and thus individual object tracking—difficult. One proposed method for mitigating this is to combine the observations in measurement space, and use this to update the "centroid state" of the collection of objects. A consequence of this process is that there is no physical reason that the centroid should itself behave as an orbiting object. This paper presents the first steps towards this type of tracking, describing the motion of the centroid as projected in measurement space.

INTRODUCTION

The multiple target tracking problem often boils down to the issue of observation assignment.[1] When there are multiple objects in close proximity, issues such as sensor resolution, sensor uncertainty, and dynamic state uncertainty make this a difficult problem. In the space flight domain, we have the benefit of natural separation over time due to differing dynamic properties of the objects. However, there is some period of time immediately following a separation event during which the objects are still too close together to sufficiently discriminate.[2] In addition, very small objects or fragments may not be consistently observable when they are alone, but could be detected while they are still clustered together—for example, the needles of Project West Ford.[3] This work is part of an overall effort to explore options for tracking clusters of objects at very early stages following the separation event. This paper specifically addresses the basic dynamics of this problem.

While this type of problem has not typically been of great consequence in this particular domain, there are other fields which require immediate tracking of groups or clusters of targets. Most literature addressing this problem stems from the missile defense community, where the problem is to track one or more targets among multiple decoy objects, or clutter, following a similar trajectory. Tracking the centroid of this group, as well as one or more parameters of cluster extent, has been proposed as a possible solution.[4,5,6] A related topic known as finite set statistics[7] attempts to address similar problems, but comprises a significantly different methodology that we will not discuss further in this paper.

At a high level, the process involves finding the geometric center of all included observations in measurement space, then using this "virtual observation" to update the centroid state of the group. Near the limit of the sensor's resolution, the centroiding may be done implicitly—two or more objects could be so close together that they present a merged target. In this case, this type of tracking could even provide information about whether, for instance, an expected deployment has already occurred or not.

*Code 8233, Naval Research Laboratory, Washington, DC 20375-5355.

This paper represents the first steps towards implementation of a centroid-based tracking and estimation framework. It addresses several fundamental aspects: the representation of the centroid itself, the dynamics of an object that represents a combination of several constituent satellites, and how these issues manifest in state and measurement space.

First, the problem of which coordinate system to use for the centroid calculation is addressed. Comparisons are made between inertial Cartesian, equinoctial elements with mean motion, and equinoctial elements with semimajor axis, as well as a relative Cartesian state. Then, two simple test cases involving a deployment of one satellite from the other are presented in order to test the performance of the various centroid methods. Finally, the results from each centroid method for a randomly-sampled deployment vector are shown, and conclusions about each method are drawn from this.

COORDINATE SELECTION

As is often the case, the coordinate system in which the centroiding is performed is expected to be critical to the accuracy of the method. To address this, we construct several simplified scenarios to explore the effects of coordinate system selection on this problem.

First, the definition of centroid—"the vector of mean values of each variable" [8, p. 225], for example—is perhaps too ambiguous for our case. The Cartesian centroid meets the typical definition for a collection of physical objects in space. However, there are more natural and convenient parameterizations of objects in orbit than Cartesian position and velocity, such as the equinoctial element set. We will examine the relationships between these representations in this section. This is done via a series of simple illustrative examples that will show the centroid's dependence on the chosen coordinate system.

To begin, consider two-body motion of two satellites in circular orbits, one with a radius of 7000 km and the other 50 km lower. At $t = 0$ they share the same angular position, that is, the lower object is directly below the higher one. In the perifocal reference frame, it is simple to represent the motion of each of these objects in two-dimensional Cartesian space:

$$x(t) = r\cos(nt) \tag{1}$$
$$y(t) = r\sin(nt), \tag{2}$$

where $n = \sqrt{\mu/r^3}$ is the angular velocity, or mean motion. The representation in polar form is:

$$r = \text{constant} \tag{3}$$
$$M(t) = nt + M_0 \tag{4}$$

where M is the polar angle (mean anomaly) and r (constant in this case) is radius.* Note that both sets of equations yield equivalent motion.

*For this example, we define M to be the angle from the $+x$ axis to the position vector.

Point centroid

Considering instantaneous points in time, the Cartesian centroid is simply

$$\overline{x} = \frac{1}{2}\sum_{i=1}^{2} x_i \tag{5}$$

$$\overline{y} = \frac{1}{2}\sum_{i=1}^{2} y_i, \tag{6}$$

and the centroid in polar form is similarly

$$\overline{r} = \frac{1}{2}\sum_{i=1}^{2} r_i \tag{7}$$

$$\overline{M} = \frac{1}{2}\sum_{i=1}^{2} M_i, \tag{8}$$

ignoring, for now, the fact that M is an angular coordinate.

Both objects, along with the Cartesian centroid (calculated at each time step), are plotted in Figure 1 for $t = 400 - 500$ seconds. The faster angular rate of the lower object is already apparent. Plotting the magnitude of the Cartesian centroid position (Figure 2), however, identifies a key problem with this methodology: the radius of the centroided orbit decreases in time. In the extreme case, when the two objects are 180° out of phase, the centroid would be nearly at the focus of the orbits. Clearly, a different treatment is required, especially for large separation distances.

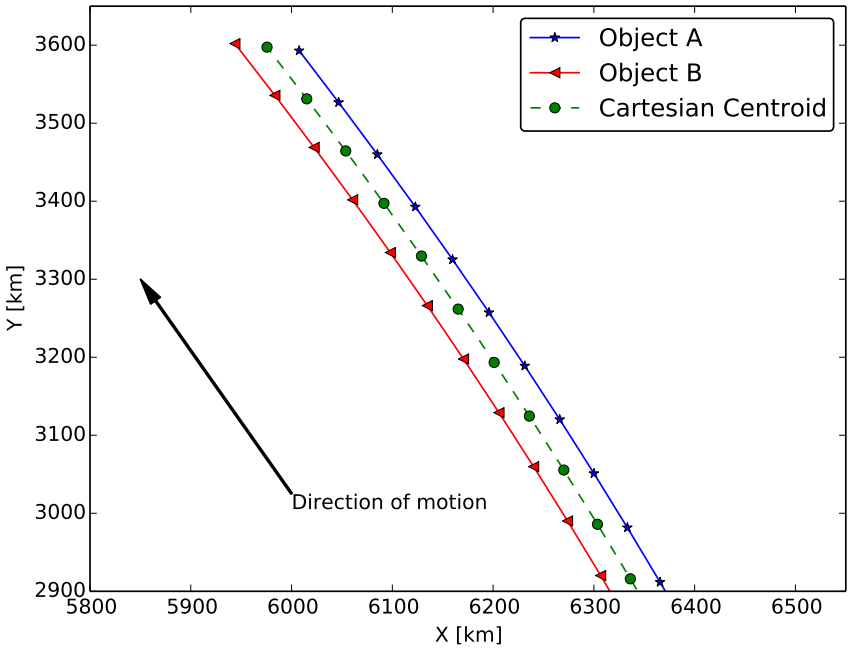

Figure 1. Cartesian centroid test case. Object A is in a higher orbit than Object B, resulting in an in-track drift.

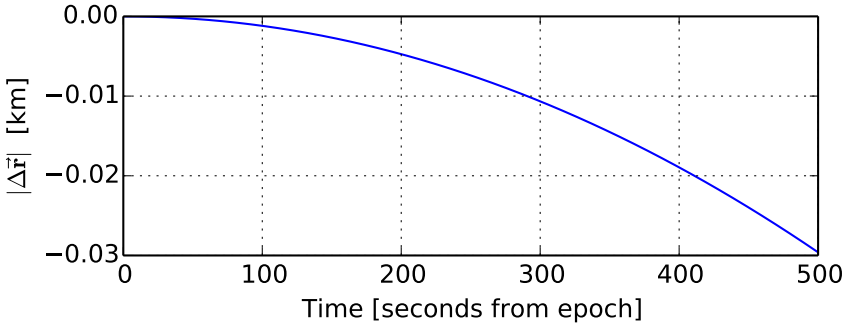

Figure 2. Change in position magnitude of the Cartesian centroid in time. Values are relative to the initial centroid radius (6975 km).

The polar form of the centroid* will have a constant radius, which is, perhaps, to be expected when averaging two circular orbits. However, the angular component must be more carefully analyzed. Consider, for instance, the average direction of 10° and 350°. For our purposes, this is 0°. However, simply averaging the two numbers 10 and 350 yields 180. To get the average direction, we use the tools of *directional statistics* [9, Ch. 2]. The mean direction of a set of angles $\{M_k\}$ is then calculated as

$$\overline{z} = \frac{1}{N}\sum_{k=1}^{N}\exp(iM_k) \tag{9}$$

$$\overline{M} = \mathrm{Arg}(\overline{z}). \tag{10}$$

When working with only two objects as we are in this paper, the benefit of this is only evident when the angular difference between the two objects is greater than 180° when measured on $[0°, 360°]$. However, when this work expands to include larger numbers and distributions of objects, treating the angular coordinate properly becomes more important, and the difference between the above method and the arithmetic mean become more pronounced.

A brief note on notation for the remainder of this paper: for some coordinate a, $\overline{a}$ is used to denote the centroid value of that coordinate, regardless of the method used, and $\mathrm{mean}(a)$ refers to the arithmetic mean operation, i.e. $\frac{1}{N}\sum_i^N a_i$.

State centroid at epoch

Because the angular rate n in Equation (4) is dependent on the radius of the orbit, calculating the centroid in polar form has two possible interpretations. In the first, the radius centroid is calculated as in Equation (7), and the resulting polar angle, now as a function of time, is

$$M(t) = \sqrt{\frac{\mu}{\overline{r}^3}}t + \overline{M}_0, \tag{11}$$

where $\overline{M}_0$ is the average of the mean anomaly at epoch of each constituent satellite, calculated with Equations (9) and (10). This formulation results in a circular orbit whose radius is the average of the two satellites.

*Alternatively, these can be thought of as "measurements" with respect to the orbit center.

Alternatively, the average *rate* could be used, in which case the centroid would be calculated as

$$\overline{n} = \frac{1}{2}\sum_{i=1}^{2}\sqrt{\frac{\mu}{r_i^3}} \tag{12}$$

$$\overline{r} = \sqrt[3]{\frac{\mu}{\overline{n}^2}}, \tag{13}$$

with the polar angle now calculated as

$$M(t) = \overline{n}t + \overline{M}_0. \tag{14}$$

Note that because $\frac{1}{2}\sum_{i=1}^{2}\sqrt{\mu/r_i^3}t \neq \sqrt{\mu/\overline{r}^3}t$ for any $t \neq 0$ (when $r_1 \neq r_2$), these two methods yield different orbits. In effect, we can either average the orbit rate, or the orbit radius (or, more generally, the semimajor axis).

First, we find the average semimajor axis centroid using Equations (7) and (11). This yields a constant orbit radius of $\overline{r} = 6975.0$ km, and a mean anomaly defined by Equation (11), with $\overline{M}_0 = 0$. Then, we can use the mean motion centroid as defined in Equation (13). The resulting orbit radius from this method is slightly lower at 6974.89 km. Each of these is used to generate a centroid orbit state at epoch that may be used for prediction and propagation. The next step is to investigate each method's performance when compared to centroided observations.

Centroid measurements are calculated by averaging the range and polar angle to each *satellite* at each time step. Then, each state space centroid is propagated, and range and polar angle to the *centroid* position are calculated. The series of centroided measurements, in effect, represents an object with average semimajor axis *and* average mean motion, which is not physically possible as the two methods vary as shown above. Thus, there will be a difference between the position derived from centroided measurements and the centroided states. The position difference between the mean measurements and each element space centroid for 1000 seconds after epoch is plotted in Figure 3.

When centroiding the angular rate, the resulting polar angle is, in fact, the mean polar angle of the two satellites. Meanwhile the radius (derived from the mean motion) is slightly offset from the mean radius of the two satellites. When the mean radius is calculated and used to define the mean motion of the centroid, however, the result is a constant drift away from the mean polar angle value, because the rates do not match exactly. This is a consequence of the nonlinear relationship between semimajor axis and mean motion. This example, while simple in construction, indicates that an orbit with an average mean motion, not semimajor axis, is likely preferable due to the absence of a secularly increasing difference. This will be discussed further with a more realistic scenario later in the paper.

Relative state centroid

We can also formulate this problem using a relative motion approach. The reference frame used here is centered on the primary satellite, and constructed by aligning the first axis with the position vector of the primary ($\hat{R}$), the third along the orbit normal ($\hat{W}$), and the second axis ($\hat{S}$) in the along-track direction, completing the triad [10, pp. 163–164]. As the orbits are circular, we can use the solutions to Hill's equations for linearized relative motion [11, pp. 84–90]. Designating the higher satellite as the primary (an arbitrary choice), the motion of the lower satellite will simply be a linear drift along the in-track axis. Centroiding in Cartesian space in the RSW frame is essentially finding

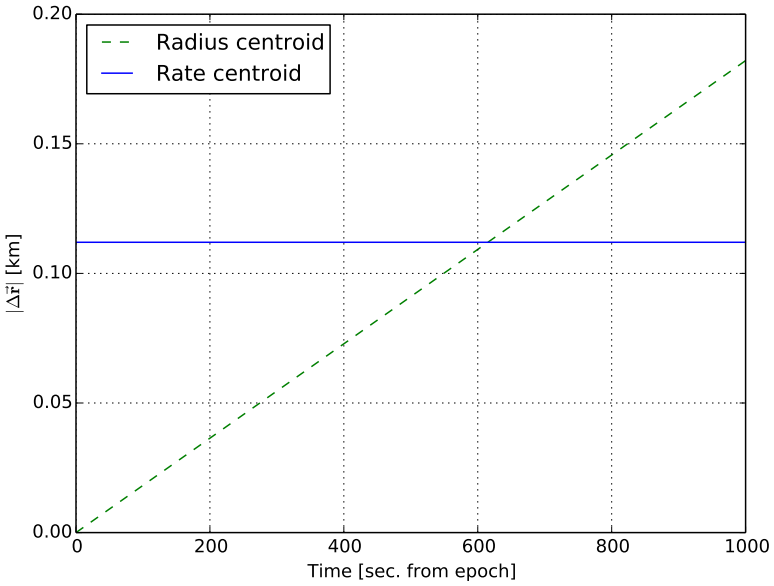

Figure 3. Position difference between measurement-space and each state-space centroid technique.

the midpoint between the second satellite and the origin, and so there are no issues *in this frame* due to the linearized motion (Figure 4). Further, in the coelliptic drift case, the in-track velocity term is a *linear* function of radial displacement ($\dot{y} = -3/2 x_0 n_{\text{primary}}$) [10, p. 403] and so the issues of averaging rate versus averaging semimajor axis do not appear here. As such, determining the centroid relative state at epoch and propagating it independently (using the solutions to Hill's equations) yields the same motion as centroiding the relative state at each time step.

It is important to remember the assumptions inherent to Hill's treatment of relative motion, however. This is only valid for near-circular orbits, and for small separation distances. After converting the centroid ephemeris back to an inertial frame, we see a departure from the initial centroid orbit radius of 6975 km, as shown in Figure 5. This is due to the linear nature of the in-track axis, and is significantly improved through the use of a *curvilinear* frame, in which the $\hat{S}$ and $\hat{W}$ axes follow the curvature of the orbit (Figure 6). [11, pp. 99–103] Note that the maximum drift in radius of about 10 cm occurs when the satellites have already separated by tens of kilometers. While the centroid orbit radius does drift in time, the relatively small magnitude and the fact that we are particularly interested in closely-spaced objects means that calculating the centroid in a curvilinear relative frame may be sufficient for our purposes. Working in this space may prove to simplify later parts of the centroid tracking problem such as centroid parameterization or estimation.

SIMULATED RESULTS

In order to further investigate the effects of centroiding, a scenario with a single ground station and pairs of satellites was constructed. Each scenario begins with the reference orbit detailed in Table 2, where $u = \omega + \nu$ is the argument of latitude, used because the orbit is circular at epoch. Most simulations include only two body dynamics, with the exception of the simulations presented in Figures 12 and 13, which also include the secular effects of the J_2 zonal harmonic. This was done

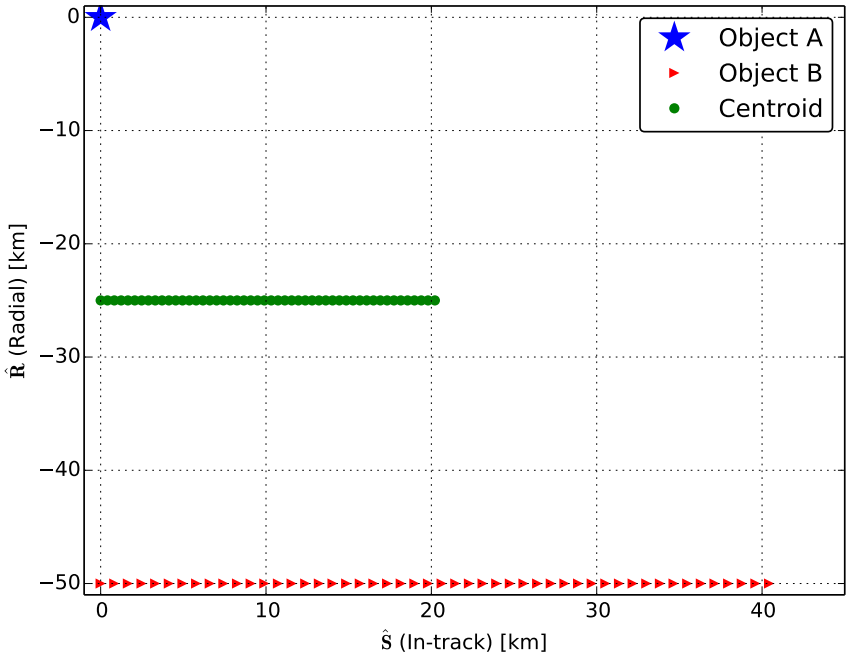

Figure 4. Cartesian centroid in the RSW frame, centered on Object A.

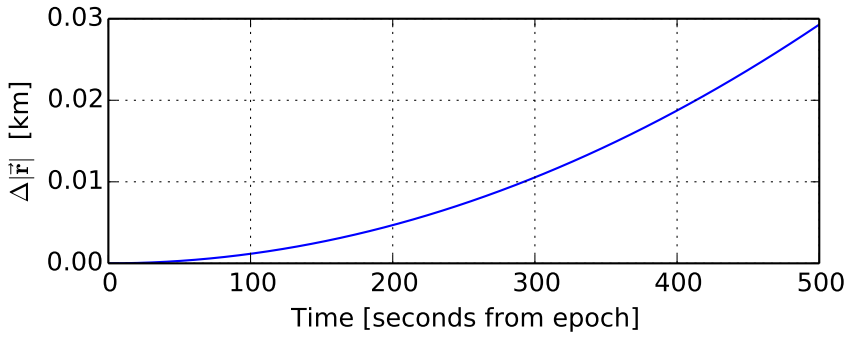

Figure 5. Drift in radius resulting from calculating the Cartesian centroid in the RSW frame.

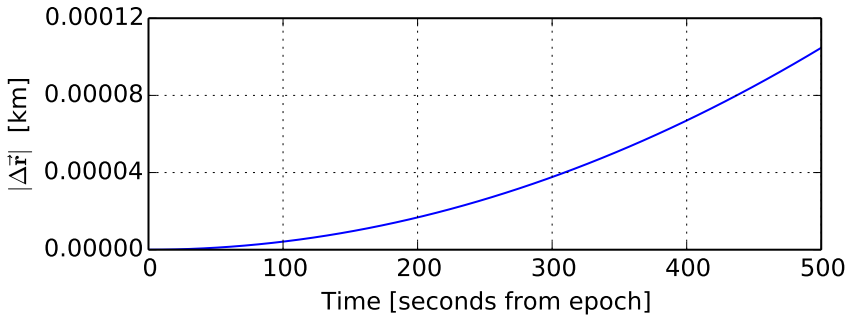

Figure 6. Drift in radius resulting from centroiding in a curvilinear relative frame.

Average semimajor axis	Average mean motion	Average relative state
$\overline{n} = \sqrt[3]{\frac{\mu}{\overline{a}^3}}$, where $\overline{a} = \text{mean}(a)$	$\overline{n} = \frac{1}{N}\sum_i^N \sqrt[3]{\frac{\mu}{a_i^3}}$	$\overline{x}^{\text{RSW}} = \text{mean}(x^{\text{RSW}})$
$\overline{a_f} = \text{mean}(a_f)$	$\overline{a_f} = \text{mean}(a_f)$	$\overline{y}^{\text{RSW}} = \text{mean}(y^{\text{RSW}})$
$\overline{a_g} = \text{mean}(a_g)$	$\overline{a_g} = \text{mean}(a_g)$	$\overline{z}^{\text{RSW}} = \text{mean}(z^{\text{RSW}})$
$\overline{\chi} = \text{mean}(\chi)$	$\overline{\chi} = \text{mean}(\chi)$	$\overline{\dot{x}}^{\text{RSW}} = \text{mean}(\dot{x}^{\text{RSW}})$
$\overline{\psi} = \text{mean}(\psi)$	$\overline{\psi} = \text{mean}(\psi)$	$\overline{\dot{y}}^{\text{RSW}} = \text{mean}(\dot{y}^{\text{RSW}})$
$\overline{\lambda}_0 = \text{Arg}\left(\frac{1}{N}\sum_k^N \exp(i\lambda_k)\right)$	$\overline{\lambda}_0 = \text{Arg}\left(\frac{1}{N}\sum_k^N \exp(i\lambda_k)\right)$	$\overline{\dot{z}}^{\text{RSW}} = \text{mean}(\dot{z}^{\text{RSW}})$

Table 1. Summary of the different centroid methods used in this paper. $\overline{a}$ is the notation for the centroid value of a regardless of how it was computed, and $\text{mean}(a)$ is the arithmetic mean value of a.

in order to allow for a better comparison with the relative motion centroid method.* Each satellite is propagated in time, and range, azimuth, and elevation measurements are taken from the ground station to both satellites simultaneously. Measurements are assumed to be perfect for our purposes, so that we do not conflate error due to the centroid method with error due to measurement noise.†

Measurements are taken for both satellites, and they are combined using separate techniques: Equation (7) for range values, and Equations (9) and (10) for the angular components. These averaged measurements are then converted back to an inertial state vector (first transformed into a line of sight vector, then an Earth-fixed vector, and finally rotated into the inertial frame). The combinaton of range and two angles allows for an exact transformation from centroided measurement to inertial position vector.

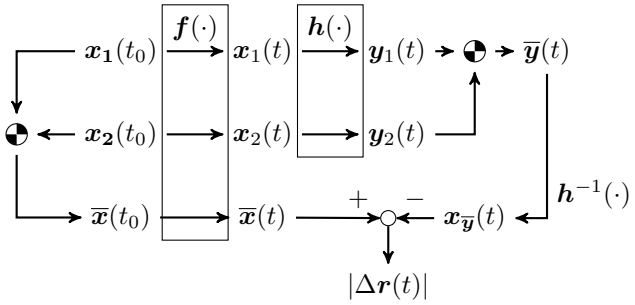

Figure 7. Diagram of the comparison process. x are object state vectors, y are measurement vectors, the ◓ symbol represents the centroiding process, $\boldsymbol{f}(\cdot)$ represents the dynamics function (i.e. propagation), and $h(\cdot)$ is the measurement function.

This averaged position vector is compared to the state vector resulting from averaging the full satellite states directly at epoch, using the three methods described above: average semimajor axis, average mean motion, and average initial relative state. The element set used for the first two is

*Future iterations of this work will utilize a relative motion theory that takes perturbations into account, such as the Gim-Alfriend geometric method. [11, pp. 150–165]

†All simulations were written in the *Julia* technical computing programming language (`http://julialang.org`).[12]

Table 2. Reference orbit used in simulations.

a	7000 km
e	0.
i	60°
Ω	175°
$u(t_0)$	0.°

the equinoctial coordinate system $(n, a_f, a_g, \chi, \psi, \lambda)$,[13] which is nonsingular except for the case of retrograde equatorial orbits. The elements (a_f, a_g, χ, ψ) are not angular coordinates, and may be averaged as in Equation (7). The mean longitude λ is of course an angular coordinate and must be handled as such by using Equations (9) and (10). Of course, calculation of the state-space centroids requires full state knowledge of all constituent satellites at epoch, which is sufficient for this work but a critical point for future studies involving estimation. As explained previously, the state-space centroid representation will be different than the one obtained by averaging in measurement space. The overall process is shown in Figure 7.

The first example involves a "deployment" shortly prior to the start of the pass, in which the secondary satellite is ejected from the primary satellite along the $-\hat{R}$ axis at 1 m/s roughly 6 minutes prior to the ground pass. The magnitude of the position difference between the measurement space centroid and state space centroids is plotted in Figure 8. As the simulated deployment is in the

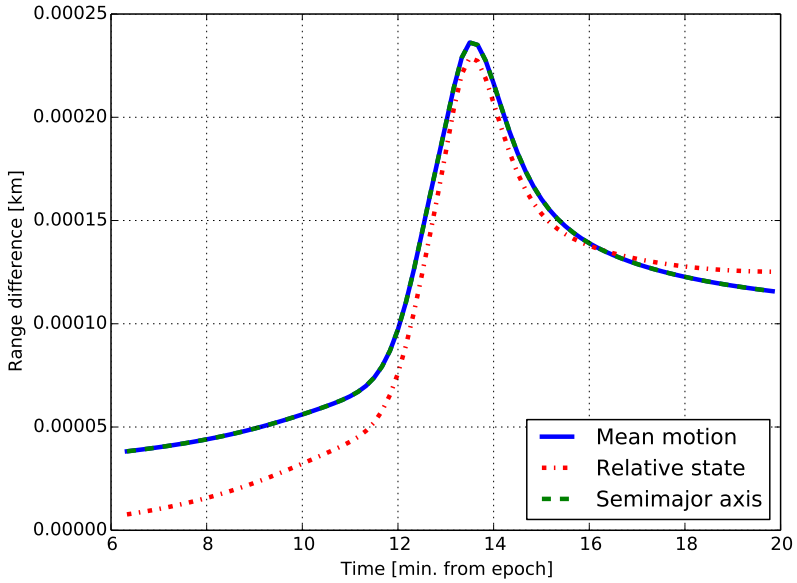

Figure 8. Difference between measurement-space and state-space centroid representations for the radial deployment scenario. The curves for average mean motion and average semimajor axis are on top of one another.

radial direction, there is no change to the semimajor axis, and so no difference between the average

mean motion and average semimajor axis methods. In all cases, the range difference begins by increasing slowly, until the satellites near peak elevation (around 86°) with respect to the ground station. Near this peak elevation, the measured azimuthal angle for each satellite is changing at a high rate, resulting in a larger azimuth angle separation. The maximum difference between the centroids is about 24 cm. Over the same pass, the true separation between satellites is about 1.6 km. In general, the error seems to grow with increasing angular separation (see Figure 9). Interestingly, while the relative state centroid exhibits the same pattern, it actually performs slightly better over most of the pass.

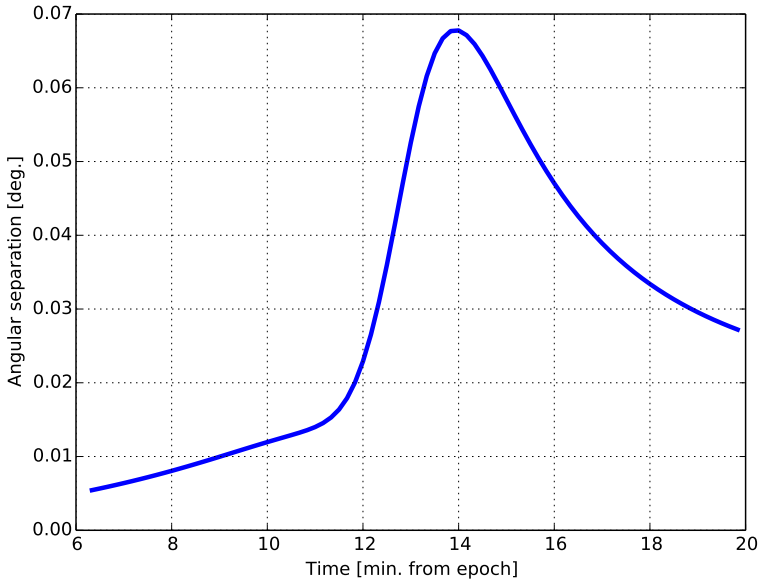

Figure 9. Angular separation between the two satellites as measured from the ground station.

A deployment in the in-track direction, on the other hand, will yield the largest difference between the two element space centroid techniques. A 1 m/s in-track deployment is simulated, and the position difference is plotted in Figure 10. As expected, there is a pronounced difference between the techniques, and the difference grows with time. The difference from the relative state centroid is the lowest at the beginning of the pass, but as the satellites drift apart the average mean motion method outperforms it. A similar dependence on angular separation is seen when averaging in mean motion, as shown in Figure 11. The peak, as in Figure 9, occurs when the satellites are near the ground station's zenith, and azimuth is changing rapidly.

The next test case is constructed to more thoroughly investigate the connection between the deployment vector and the centroid error. Here, 1000 deployment vectors are generated at random, while the magnitude of the deployment remains constant at 1 m/s. The same centroiding techniques described above are used, and the maximum range error (between measurement-space and element-space centroids) is mapped to color on the unit sphere in Figures 12, 13, and 15. The two element-space centroid cases were performed with a propagator that includes the secular effects of J_2, and the relative state space centroid case includes only two-body motion.

First, we look at the error resulting from averaging the semimajor axis of the two satellites at

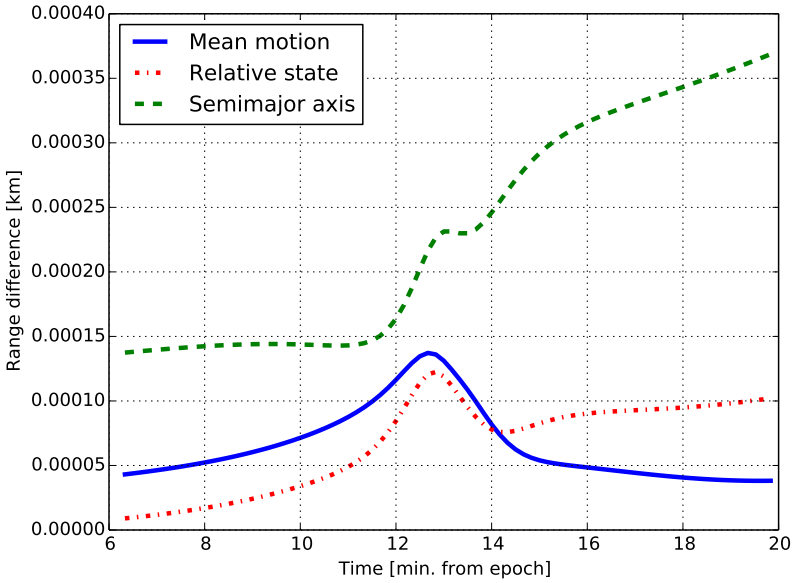

Figure 10. Magnitude of the difference between the position vector derived from centroided measurements and those derived from the state-space centroids for the in-track deployment scenario.

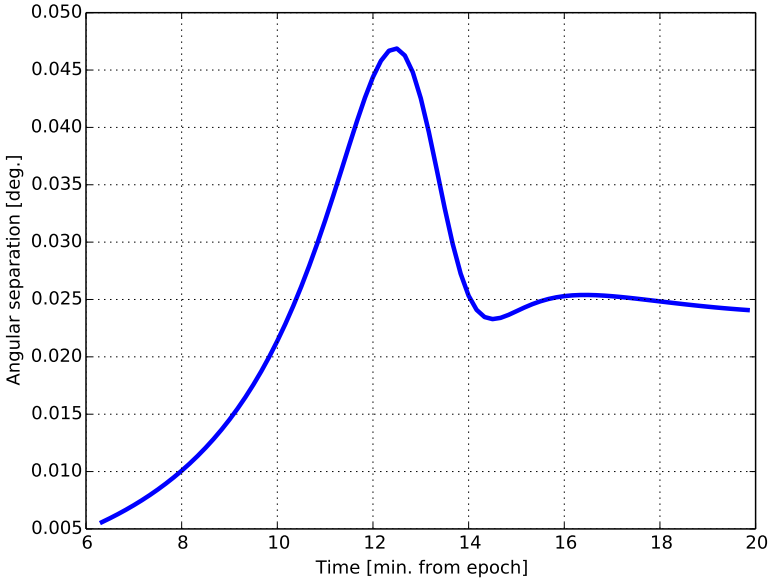

Figure 11. Angular separation between the two satellites as measured from the ground station for the in-track deployment scenario.

epoch (Figure 12). The reference axes in the figure correspond to the RSW frame. The maximum position difference, in this case, occurs when the deployment vector is roughly along the $\hat{S}$ axis, or along-track. This corresponds to a greater increase in semimajor axis, and a higher difference between the two centroid methods. Referring back to Figure 3, we can see that averaging semimajor axis leads to a secular drift (in-track), away from the measurement-space centroid.

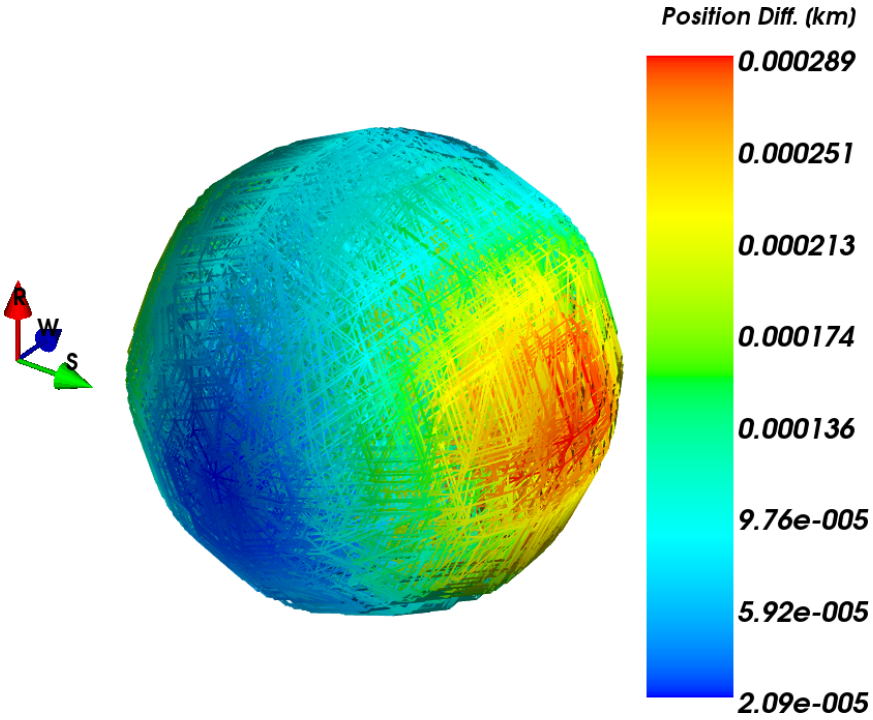

Figure 12. Maximum position difference between measurement-space and state-space (using semimajor axis) centroids for a randomly-chosen deployment vector. The red axis is $\hat{R}$, $\hat{S}$ is in green, and $\hat{W}$ is the blue axis.

Figure 13 shows the result of averaging the mean motion of the two satellites at epoch. First, note that the maximum position error here is an order of magnitude lower than that in Figure 12. Here, error is highest when the deployment vector is along the $\hat{R}$ axis. To understand this, first note that radial deployment vectors result in the smallest change in semimajor axis. Thus, the difference between the two centroid methods is smallest for these directions. The error in this case, then, is simply driven by the angular separation (as shown in Figure 9). Figure 14 illustrates this for the randomly sampled deployment vector case. Larger angular separations over the pass occur near the $\hat{R}$ axis, corresponding to the higher error at these deployment directions.

Finally, Figure 15 shows the result of averaging in relative state space at epoch. The magnitude of the position difference is similar to the average mean motion centroid. However, the deployment vector at which this difference is maximal is at about 45° off-zenith in the orbit plane. Referring to Figure 14, this does not quite correspond to peak angular separation. Plotting a radial, in-track, and 45° off-zenith deployment in the relative frame (Figure 16) lends some insight. The plot indicates that the deployment vector midway between the $\hat{R}$ and $\hat{S}$ axes leads to the largest Euclidean separation between the two satellites. Indeed, when plotting this maximum distance for all samples in Figure 17, the same trend as in Figure 15 is evident. This indicates the error when using relative

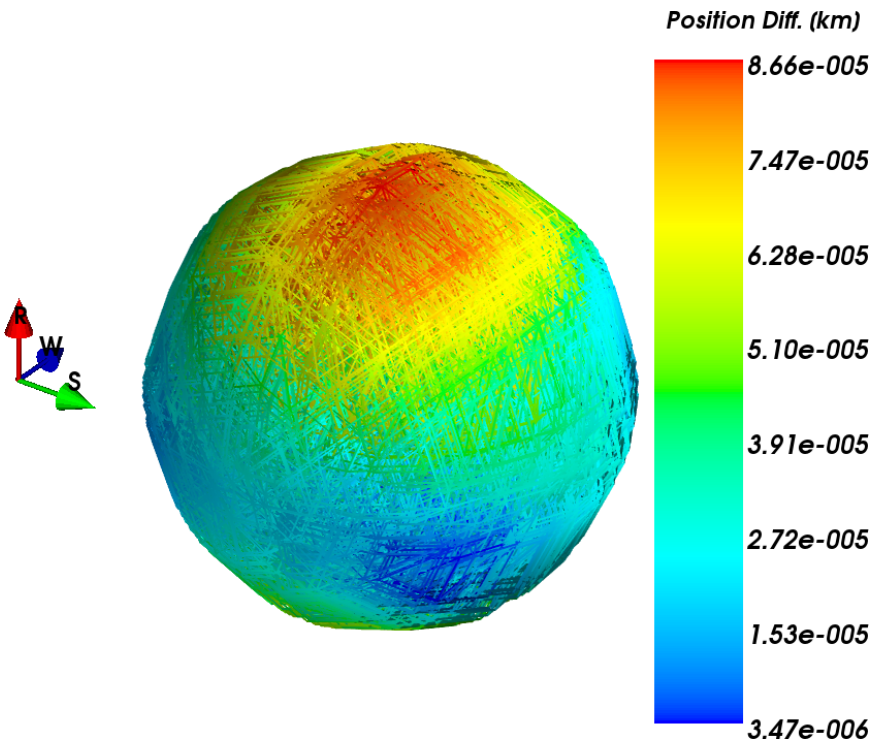

Figure 13. Maximum position difference between measurement-space and state-space (using mean motion) centroids for a randomly-chosen deployment vector.

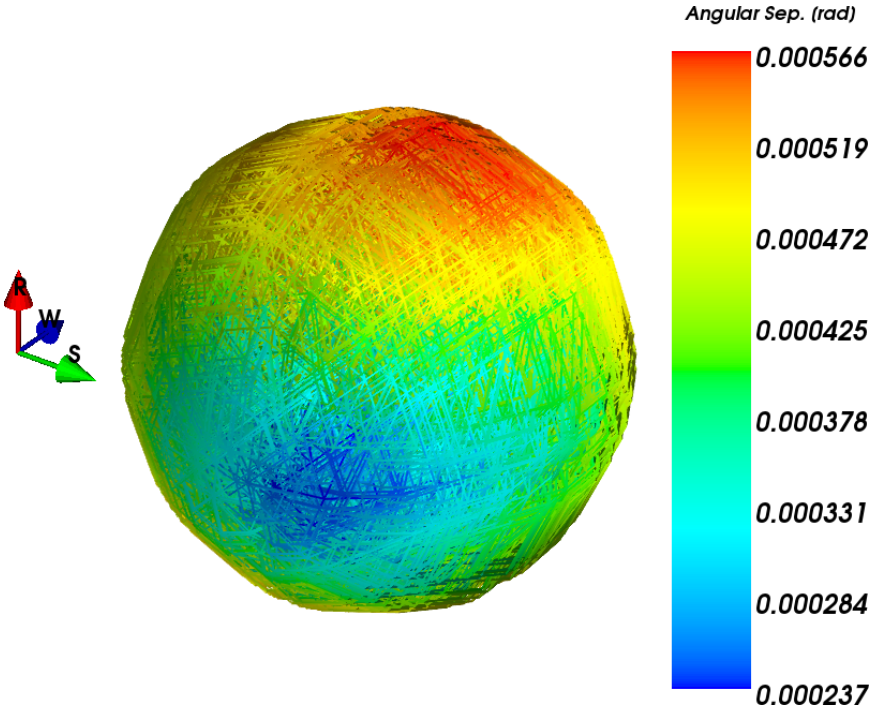

Figure 14. Maximum angular separation between satellites for a randomly-chosen deployment vector.

state space centroiding is driven by the Euclidean distance between satellites. Note that this distance also affects the validity of the assumptions that go into using the solutions to Hill's equations for propagation.

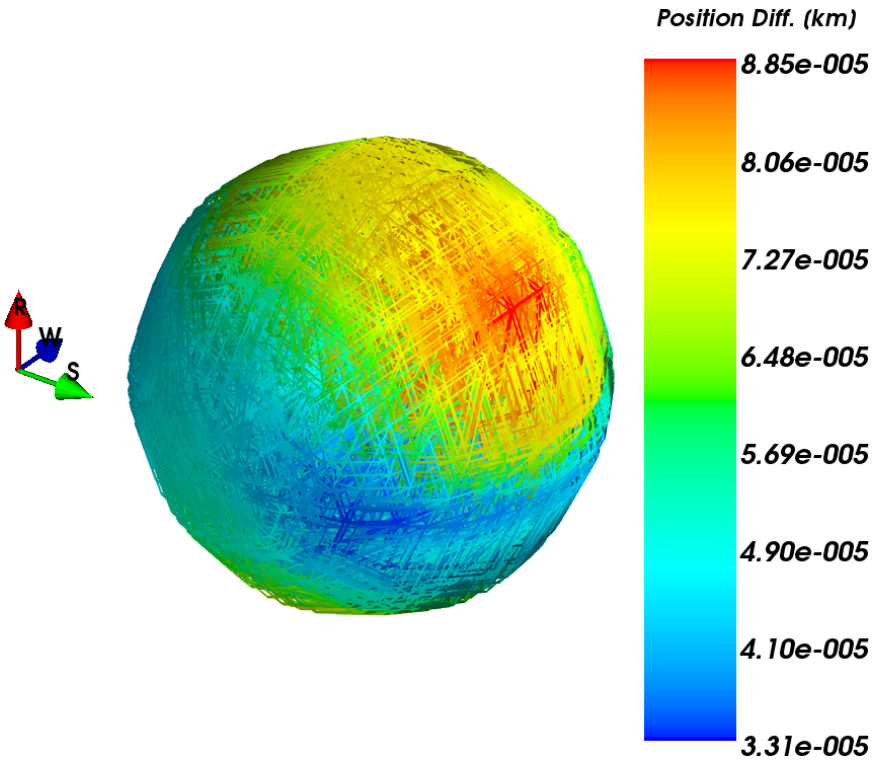

Figure 15. Position difference between measurement-space and relative state-space centroids for a randomly-chosen deployment vector.

As an interesting side note, the results presented in Figures 14 and 17 indicate preferred deployment vectors for mission designers who wish to induce maximum separation. Angular separation is likely most desirable from the standpoint of discrimination and identification, although of course the trajectory resulting in the maximum angular separation immediately post-deployment (along the $\hat{R}$ axis) will return to a point near the original deployment one orbit later. The preferred direction in Figure 17, changes the energy of the orbit, ensuring a secular drift along-track and still resulting in a modest angular separation immediately post-deployment.

Ultimately, this work will be applied to the tracking and estimation problem. If the centroid state is being tracked and updated using centroided measurements, we know that at least one measurement component will exhibit systematic error. For instance, using a centroided mean motion state representation, the Coordinate Selection section shows that the range component will be biased, albeit in a predictable way. This is likely preferable to the centroided semimajor axis approach, in which the angular separation grows in time. In any case, this work suggests that different types of measurements be handled in different ways. As an example, perhaps estimation is first performed using angles measurements only. Then, with better knowledge of the centroid mean motion, the range measurements could be de-biased before processing.

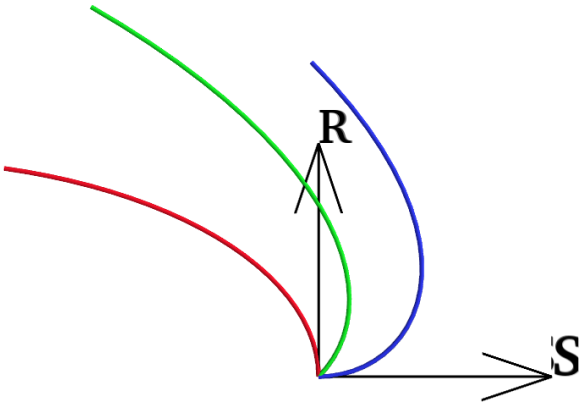

Figure 16. Sample relative trajectories over the ground pass. A radial deployment is shown in red, an in-track deployment in blue, and a 45° off-zenith in green.

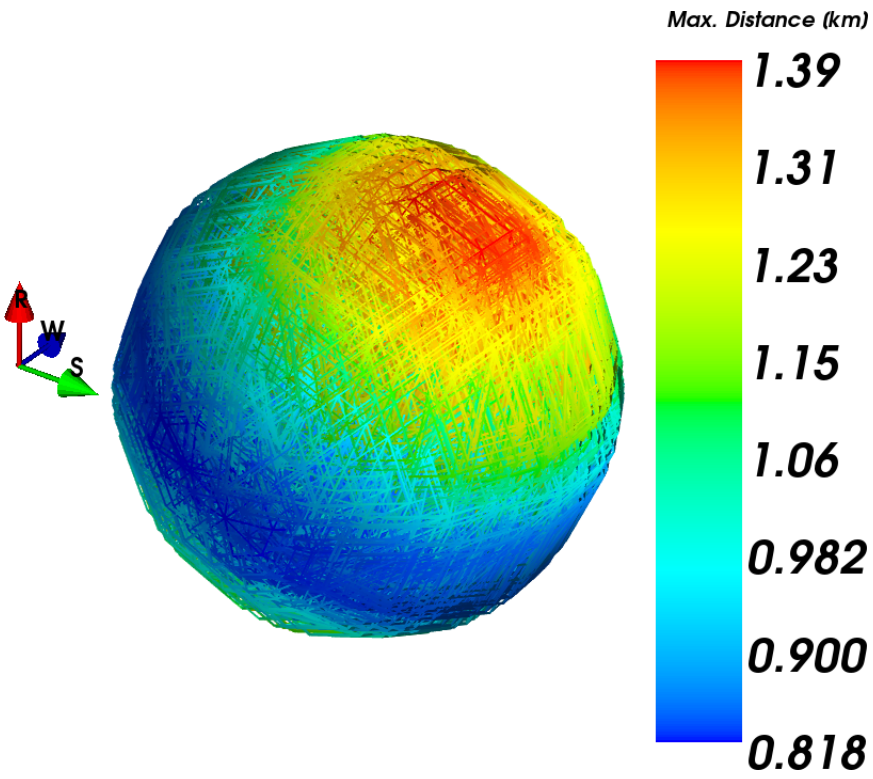

Figure 17. Maximum distance between the two satellites for a randomly-chosen deployment vector.

Measurements would be combined (after the proper gating* steps) in measurement space, then used to update knowledge of the state-space centroid. This avoids the problem of observation association that currently limits the tracking process for closely-spaced objects. Additionally, the pre-centroided measurements contain information about the "spread", or extent, of the target cluster. The cluster extent would be parameterized in some way (this could be something analagous to a covariance matrix), and the relevant parameters would be updated as part of the estimation process.

SUMMARY AND CONCLUSIONS

Calculation of the centroid is coordinate system dependent. The coordinate system comparison clearly shows that inertial Cartesian coordinates do not work well for characterizing centroid dynamics. The choice of orbit energy parameterization (semimajor axis or mean motion), however, is not as immediately evident. The test cases presented here indicate that averaging mean motion will be more consistent with observations, particularly for longer propagation times. Additionally, under certain conditions, the relative state centroid yields similarly promising results.

Centroided measurements represent, in effect, an object with both average semimajor axis and average mean motion, which is not possible unless the two objects have the same energy. As such, there is a difference when comparing state space centroids with centroided measurements. When comparing these two, patterns emerged between the deployment vector and the error magnitude. This error varies systematically according to the geometry of the problem. When averaging semimajor axis, error is maximal when the deployment vector is near the in-track direction, i.e. when the difference in orbit energy between the two satellites is highest. When averaging mean motion, error is driven primarily by the angular separation of the two satellites. Finally, the relative state centroid error is driven by the Euclidean distance between objects. These results lend insight to more general cases beyond the deployment scenario. From another perspective, the plots showing maximum angular separation and Euclidean distance could be used by a mission designer to help choose the deployment vector.

From these results we can draw several conclusions. Foremost, calculating the centroid by simply averaging the equinoctial elements with semimajor axis is insufficient to capture the true dynamics as they manifest in measurement space. Using the equinoctial element set with mean motion as the orbit energy component, however, results in fairly good performance when compared to the measurements, with a maximum error of $< 0.01\%$ of the maximum Euclidean distance in the scenarios presented here. Finally, the average relative state, propagated using the solutions to Hill's equations, can be sufficient to capture the proper dynamics of the centroid, at least in the restricted cases presented here.

FUTURE WORK

As this paper represents only the first step towards a comprehensive way of tracking objects as a cluster, there remains a significant amount of work to be done. A larger number of satellites should be centroided in order to ensure the general findings of this paper are consistent. A wider range of cluster geometries should be explored to find possible limitations of both the equinoctial state space and relative state space approaches.

*Gating is the preliminary process of determining if a measurement should be considered as being *possibly* associated with the target(s) of interest. See Blackman and Popoli[6] and Binz and Healy[1] for more details.

One other potential application of this work could also prove useful. In the case of observations that are unable to be distinguished (a "merged observation"), either due to poor sensor resolution or close proximity, this work could provide a way to indicate the presence of more than one object. For instance, perhaps the presence of a deployed object or an object otherwise in close proximity to the known object could be detected simply by observing the residuals.

As discussed previously, the cluster extent needs to be parameterized in some way, a possible subject of its own future paper. This is one specific area in which a linearized relative motion approach could be beneficial. Once these issues have been worked out, the actual problem of tracking and estimation needs to be addressed. Finally, tracker performance based on realistic scenarios and data should be characterized.

REFERENCES

[1] C. Binz and L. Healy, "Association of satellite observations using Bayesian inference," *Spaceflight Mechanics 2013*, Vol. 148 of *Advances in the Astronautical Sciences*, San Diego, CA, Univelt, Inc., 2013. AAS 13-245.

[2] A. Segerman, J. Byers, J. Emmert, and A. Nicholas, "Space Situational Awareness of Large Numbers of Payloads From a Single Deployment," *2014 AMOS Technical Conference, Wailea, Maui, HI*, 2014.

[3] D. MacLellan, W. Morrow, and I. Shapiro, "Effects of the West Ford belt on astronomical observations," *Proceedings of the IEEE*, Vol. 52, May 1964, pp. 564–570, 10.1109/PROC.1964.2996.

[4] M. A. Zimmer and M.-J. Tsai, "Tracking of a single cluster of closely spaced objects using one and two passive optical sensors," *Signal and Data Processing of Small Targets 1992*, Proc. SPIE, International Society for Optics and Photonics, 1992, p. 268–280, 10.1117/12.139378.

[5] M. A. Kovacich, T. Casaletto, W. E. Lutjens, D. D. McIntyre, R. Ansell, and E. VanDyk, "Application of MHT to group-to-object tracking," *Signal and Data Processing of Small Targets 1991*, Proc. SPIE, International Society for Optics and Photonics, 1991, p. 357–370, 10.1117/12.45669.

[6] S. Blackman and R. Popoli, *Design and Analysis of Modern Tracking Systems*. Norwood, MA: Artech House, Inc., 1st ed., 1999.

[7] R. P. S. Mahler, "Detecting, tracking, and classifying group targets: a unified approach," *Proc. SPIE*, Vol. 4380, 2001, pp. 217–228, 10.1117/12.436950.

[8] E. D. Feigelson and G. J. Babu, *Modern Statistical Methods for Astronomy: With R Applications*. Cambridge University Press, July 2012.

[9] K. V. Mardia and P. E. Jupp, *Directional Statistics*. John Wiley & Sons, Inc., 1999.

[10] D. A. Vallado, *Fundamentals of Astrodynamics and Applications*. Hawthorne, CA: Microcosm Press, 3rd ed., 2007.

[11] K. Alfriend, S. R. Vadali, P. Gurfil, J. How, and L. Breger, *Spacecraft Formation Flying: Dynamics, control and navigation*. Butterworth-Heinemann, Nov. 2009.

[12] J. Bezanson, S. Karpinski, V. B. Shah, and A. Edelman, "Julia: A Fast Dynamic Language for Technical Computing," *arXiv:1209.5145 [cs]*, Sept. 2012. arXiv: 1209.5145.

[13] J. R. Wright, "LS GEO IOD," *The Journal of the Astronautical Sciences*, Vol. 59, June 2012, pp. 352–369, 10.1007/s40295-013-0022-5.